The 2009 IEEE/RSJ International Conference on
Intelligent Robots and Systems
October 11-15, 2009 St. Louis, USA

Develop Feedback Robot Planning Method for 3D Surface Inspection

Quan Shi, Chi Zhang, Ning Xi, and Jing Xu

Abstract— **The non-contact 3D sensing technology, though achieved many success in a variety of applications, needs an automation system to expand its applications to automotive industries for 3D shape inspection. The reason is the difficulty for an operator to find an optimal solution by the manual control of sensor viewpoints. The problem of this industrial application is the capability for the sensing system to simultaneously satisfy all requirements of competence, efficiency, and cost. A robot-aided 3D sensing system can provide such a solution. A CAD-guided robot view planner can automatically generate viewpoints. Measurement accuracy can be satisfied in a certain range. However, the unpredictable image noises still need to be compensated for better measurement performance. In this paper, a feedback planning system is designed and applied to the CAD-guided robot sensor planning system. The feedback controller can automatically evaluate the accuracy of obtained point clouds and generate new viewpoints. This feedback-based inspection system had been successfully implemented in filling holes of a point cloud, caused by shadows and light reflections. Such a system had been implemented on an ABB industrial robot for a 3D measurement of an automotive glass and a pillar. This paper introduces the developed planning system and our current results.**

I. INTRODUCTION

The automotive industry has been seeking a rapid 3D shape measurement system for dimensional inspection. Today, many commercial 3D sensors and systems are available. However, there are still "barriers" to the adoption of 3D-based machine vision systems in the automotive industry: "Cost, Complexity, Reliability, Data Confidence, and Skilled Labors (for maintenance and support)"; and the "primary drivers for the end-user to use 3D vision are the need to lower costs and improve quality through automation", according to Nello Zuech's report with several industrial professionals in 2007. [1]. Basically, for non-contact measurement, it is difficult for a human operator to move the robot for a satisfied measurement performance. Robot planning and control may provide a solution: a robot sensor planner can enhance the measurement quality and efficiency. Therefore, view planning has been an active research area in robot automation and becomes more important in the area of 3D surface measurement and inspection.

Previous research on automatic view planning for visual inspection can be found in [2] and [3]. Most of previous works focused on planning a laser scanner because white light area sensors were generally bulky and heavy to be mounted on a robot. Chen and Li developed white-light area sensor planning using model-based view planning approach [4]. Though the projector is fixed, Chen developed an equivalent sensing model to couple the constraints of a pair of cameras mounted on a robot hand. This approach gives a comprehensive analysis of the planning constraints, but the illumination condition is not integrated because the projector is fixed. Indeed, illumination problem is a serious problem for white-light area sensor. Generally, white-light area sensors can only measure a lambertian/diffuse surface. A shiny surface, caused by specular reflection, still needs a pretreatment such as a powder spray before 3D measurement. Besides, the shape complexity generates occlusion problem that appears shadows on the part surface. To solve these signal dynamic range problem, Qian proposed a novel sensor planning approach based on spherical mapping, geometrical reasoning, and an iterative optimization strategy [5]. Qian's approach, has an advantage to avoid the illumination problem in planning stage. Another approach, proposed by Impoco et. al in 2004, is to compensate the problem by adding additional viewpoints through clustering unseen directions [6]. Impoco's method is more practical, and the computation of additional viewpoints based on the measured point cloud is straight forward. Besides, the additional viewpoints can be used to improve the measurement performance. Although the robot path may not be efficient, it is tolerable for an industrial application.

Intensity noise is often a random noise in the process of counting photon energy for each pixel. This type of noise mainly depends on the image grabbing system and can be reduced using filtering techniques. Another type of error from the image is the quantization error [7][8], which is unavoidable in many vision systems. Therefore, a high resolution camera is usually required for better accuracy. Besides, with a same camera, a proper viewpoint can also be used to reduce this quantization error [9]. Third, the surface property of light reflection is a problem particularly when a projector is involved in a vision system. Because various materials have different reflection properties, the projected patterns may not be clearly recorded. For example, in a low contrast region of an image, error is often increased because the edge of projected fringes becomes easy to be noised.

Feedback-based view planning method is a possible solution to solve those problems. A prototype 3D area sensor had been developed previously [10], this paper specially focus on the measurement optimization through view planning method. The measured point clouds and collected images can be used to identify problem regions and estimate new

The work described in this paper is supported under NSF Grant IIS-9796300, IIS-9796287, EIA-9911077, DMI-0115355, and FORD Motor Company University Research Program.

Q. Shi is with Glass Research at PPG Industries Inc. Cheswick, PA. 15024, USA. qshi@ppg.com

C. Zhang, N. Xi, and J. Xu are with the Department of Electrical and Computer Engineering, Michigan State University, East Lansing, MI. 48823, USA. zhangc11@egr.msu.edu

viewpoints to cover that. The principle of this feedback-based view planning system is: two measurements are conducted on a part surface, the variations of the measured shape are analyzed such that new viewpoints can be generated to improve the measurement accuracy. Particularly, when a low contrast area is detected, a new viewpoint can then be generated to cover that part of surface. Although the processing time of this feedback-based system is much longer than a CAD-guided view planning system, the measurement accuracy will be improved, which is indeed required for industrial applications.

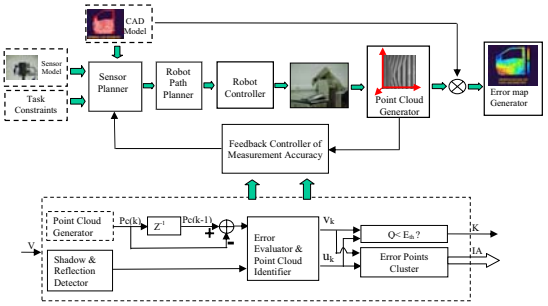

Fig. 1. A feedback-based robot sensor planning system for rapid 3D shape inspection

A dynamic view planning system and the specific feedback controller is shown in Figure 1. The goal of this dynamic planning process is not only to build an automatic inspection system, but also improve the measurement quality.

II. CAD-Guide Robot Planning

A CAD-guided area sensor planner is developed to estimate a preset of robot viewpoints. Five constraints are usually need to be considered: visibility, field of view, resolution, point density, and depth of focus. Different from planning a single camera, constraints of both camera and projector have to be satisfied. As shown in Figure 2, V is the vector of sensor viewing norm, V_{avg} is defined by the average norm of a patch of surface. C_1, C_2 are vectors of camera viewing normal constraints, and P_1, P_2 are vectors of projection normal constraints. S_1, S_2 are vectors of surface normal constraints that are limited by C_1, P_1 and C_2, P_2. This constraint ensures that this patch surface can be illuminated by projector and images of this patch surface can be taken by camera. Threshold angles of θ_1 and θ_2 are used to define visibility constraints and angle θ_{tri} represents the angle between any single triangle and the surface average norm, as shown in Eqn. (2).

$$\begin{aligned} \theta_1 &= \arccos\left(\frac{S_1 \cdot V_{avg}}{\|S_1\|\|V_{avg}\|}\right) \\ \theta_2 &= \arccos\left(\frac{S_2 \cdot V_{avg}}{\|S_2\|\|V_{avg}\|}\right) \\ \theta_{tri} &= \arccos\left(\frac{V_{tri} \cdot V_{avg}}{\|V_{tri}\|\|V_{avg}\|}\right) \end{aligned} \quad (1)$$

$$|\theta_{tri}| < \begin{cases} |\theta_1|, & sign(\theta_{tri}) = sign(\theta_1) \\ |\theta_2|, & sign(\theta_{tri}) = sign(\theta_2) \end{cases} \quad (2)$$

The given CAD model is first tesselated into triangles. Then,

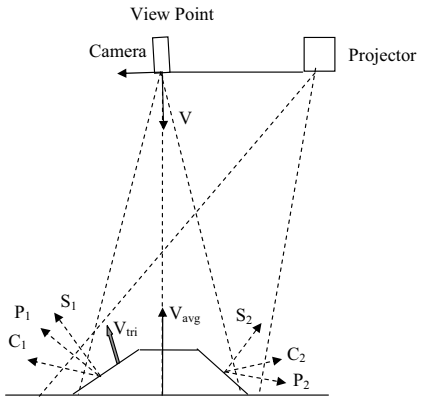

Fig. 2. Deriving visibility constraints of an area senor

based on the normals and areas of triangles, a clustering algorithm was used to separate all triangles into a set of smooth patches.

The other constraints are described as follows:

1) Field of view determines the size of maximum inspection area. It is usually a rectangular field. In the developed Area sensor planner, it was determined by the standoff and camera viewing angles.
2) Resolution defines the entity's minimal dimension to be mapped onto one camera pixel.
3) Point density is a constraint determined by the field of view and the resolution of the projector, which is a new constraint developed for the automated Area sensor planning system. Point density constraint ensures that enough points can be measured for certain area of surfaces.
4) Focus constraint defines the farthest measurement distance and the nearest measurement distance from a viewpoint.

A bounding box method is developed to integrate all constraints of both a camera and a projector for searching viewpoints. Illustrated in Figure 3, a candidate patch is concluded in a bounding box, the width and the length of the box specify the field of view and the height of the box specifies the farthest and nearest focus distances. A viewpoint can be estimated on the center line that passes through the bounding box.

$$\min_{\vec{P}} \sum_{i=1}^{N} F(C_{i1}, C_{i2}, ..., C_{i5} \in R_c \mid P_{i1}, P_{i2}, ..., P_{i5} \in R_p) \quad (3)$$

III. Feedback Robot Planning

A. Measurement error analysis

A gray coded line shifting (GCLS) method had been applied to our 3D area sensor [10]. Precisely determining the boundary of strips is a critical issue for a successful 3D

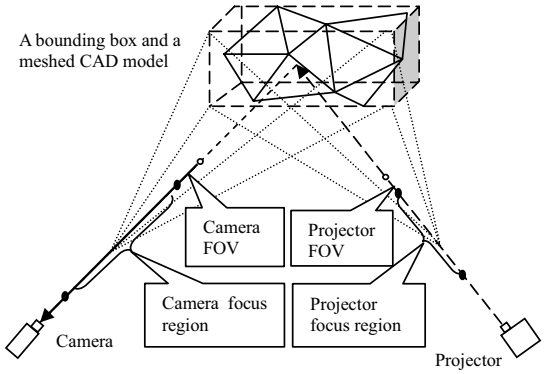

Fig. 3. Integration of planning constraints using a bounding box method

shape measurement. To calculate the depth from one surface point to a pre-calibrated reference, edges of strips have to be calculated in sub-pixel resolution. If not, quantization error will be added into measurement results. As shown in Figure 4, the edge of a stripe can arbitrarily fall in any place between an image pixel n and its next pixel $n+1$.

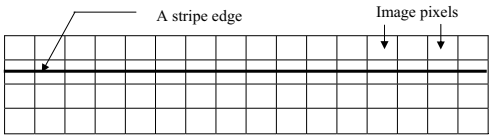

Fig. 4. Image quantization error in edge detection

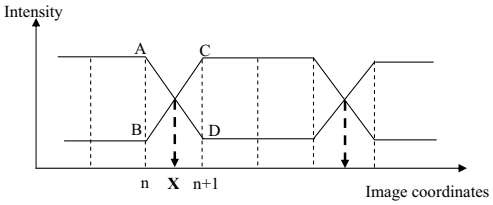

Fig. 5. Edge detection using interpolation strategy

To estimate the location of the stripe in sub-pixel accuracy, an edge detection method is used, as shown in Figure 5: using another image with opposite intensity stripes, A, B, C, and D represents four intensity values that will be used to calculate X, the location of a stripe boundary. Sub-pixel accuracy can be achieved with this interpolation calculation.

The estimation of X may have error because of image noises, but it is bounded in one pixel. On a view surface that has a norm parallel to the viewing direction, resolution is often defined by the size of a piece surface projected onto one pixel. This resolution is a constraint widely used in many view planning system. For a freeform surface, it may contain many small patches, norms of each small patch will be vary so that the resolution of each patch is quite different. Average norm of all small patches, can be used to determines a viewpoint for those patches. This method only satisfies the global resolution constraint. However, for a small patch under that viewpoint, the angel between the surface norm and the viewing direction may exceed the threshold such that the resolution constraint cannot be satisfied. Hence, the one pixel error bound will be increased and the measurement uncertainty will not be tolerant. For surface shape inspection, this small area needs a new viewpoint to satisfy the measurement constraints.

In another aspect, measurement uncertainty can also be generated in low contrast images. Considering intensity noises, stripes in a high contrast area will be more robust than stripes in a low contrast area, which makes feedback robot planning strategy critical in solving this type of problem.

B. Mathematic model of the feedback-based inspection process

This feedback system has a CAD-guided sensor planner that can initially setup a set of viewpoints in the open-loop. A feedback controller was designed to add a set of viewpoints recursively according to the quality of the obtained point clouds. The diagram of the whole feedback-based inspection system can be seen in Figure 6. The purpose of the feedback controller is to improve the measurement accuracy.

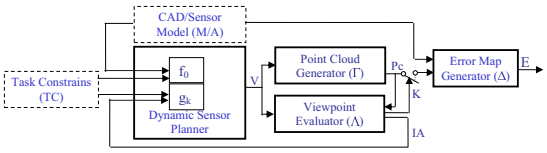

Fig. 6. Block diagram of a feedback-based dynamic shape inspection system

C. The control model of the feedback planning system

The dynamic sensor planner need various inputs such as CAD model and point cloud information. According to each type of input, viewpoints will be generated and be added into a robot path. Except the area sensing model, the dynamic sensor planner has three more inputs: 1) CAD model, 2) task constraints, and 3) feedback information.

CAD model M is usually a group of triangles tessellated from part surfaces. Mathematically, it can be represented by:

$$M = \{T_i | T_i =< (X_{i1}, Y_{i1}, Z_{i1}), (X_{i2}, Y_{i2}, Z_{i2}), (X_{i3}, Y_{i3}, Z_{i3}) >, i = 1...n\} \quad (4)$$

Task constraints TC is a set of measurement requirements, which integrate the requirements for CAD-based planning strategy and feedback-based planning strategy:

$$TC = \{fov, S, \rho, f_d, \eta, \Sigma, \sigma\} \quad (5)$$

where the field of view fov is defined by the length L and width W of a rectangle area; S is the standoff distance of an area sensor; ρ represents the image resolution; f_d represents the focus distance which contains two values: nearest focus distance, and farthest focus distance; η represents visibility of the area sensor, determined by three vectors: projection

vectors $\overrightarrow{PV}$, camera viewing vector $\overrightarrow{CV}$, and surface norm vector $\overrightarrow{SV}$. A piece of surface is visible if the following equation is satisfied:

$$\begin{cases} \arccos(\frac{\overrightarrow{PV}\cdot\overrightarrow{SV}}{||\overrightarrow{PV}\cdot\overrightarrow{SV}||}) < \theta_{th1} \\ \arccos(\frac{\overrightarrow{CV}\cdot\overrightarrow{SV}}{||\overrightarrow{CV}\cdot\overrightarrow{SV}||}) < \theta_{th2} \end{cases} \quad (6)$$

where θ_{th1} ensures that the encoded patterns can be projected onto the surface and θ_{th2} ensures that this piece of surface can be "seen" by camera. Σ represents the area of holes generated by shadows or light specular reflections. Stripes are totally lost in this part of area and the number of correspondent pixels are counted to determine the size of holes; σ is the standard deviation of measurement variations, calculated on same surfaces within two measurements. Ideally, the shape of those two point clouds should be identical. However, image quantization error and poor surface reflection property will increase the measurement uncertainties. Then, stand deviation of the differences of two measurements can be used to show how the two point clouds are vary from each other. If σ is larger than a predetermined threshold, another viewpoint then need to be set for this area.

Feedback information contains the analysis results of the measured point clouds, which is generally an inaccuracy map IA, described in Equation 7, p_i represents a 3D point in a region which has quite different shape between two measurements, ka represents the number of points in this region, and σ_{th} is a threshold value predefined as the requirement of measurement accuracy.

$$IA = \{p_i(x_{ai}, y_{ai}, z_{ai}) | i = 1, 2...ka, sigma > sigma_{th}\} \quad (7)$$

Measurement error usually is not evenly distributed over a point cloud [10]. For a single surface point, the measurement accuracy is related to the sensor viewpoint. The accuracy map IA can effectively show the differences between the measurements on two viewpoints.

Viewpoints are the output of this dynamic sensor planner. A viewpoint includes a location p and a viewing vector v. As shown in Equation 9, V_0 represents the initial set of viewpoints generated from CAD model, V_k represents the sets of viewpoints estimated in feedback, k represents the iteration times.

$$\begin{aligned} V_0 &= \{\Psi_{0i} = (p_i, v_i), p_i \in R^3, v_i \in R^3\} \quad (8) \\ V_k &= \{\Psi_{ki} = (p_{ki}, v_{ki}), p_{ki} \in R^3, v_{ki} \in R^3\} \\ V &= (\bigcup_{k=1}^{n} V_k) \bigcup V_0 \end{aligned}$$

The developed dynamic sensor planner also has two functions:

1) Initial viewpoint configuration f_0: An initial viewpoint configuration is a process to estimate viewpoints based on the given CAD model of a part. Function f_0 represents a bounding box algorithm developed to find a viewpoint set V_0 from CAD model M.

$$f_0 : M \mapsto V_0 \quad (9)$$

2) Feedback-based viewpoint configuration g_k: g_k is a projection from a defect map IA to new viewpoints.

$$g_k : IA \mapsto V_k \quad (10)$$

The viewpoint evaluator Λ is a function, which makes a decision about if the quality of a point cloud Pc satisfies the measurement requirement. If not, defect map IA will be fed back to the dynamic sensor planner to update set V.

$$\Lambda : V \mapsto IA \quad (11)$$

where viewpoint set V is the input to Λ. Figure 7 illustrates

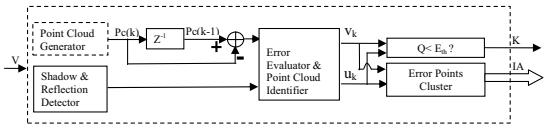

Fig. 7. Block diagram of the feedback controller, viewpoint evaluator Λ

the detail structure of this function. Two point clouds will be measured sequentially. Differences between those two point clouds will be input to the error evaluator. Meanwhile, an image processor is designed to identify the area with intolerant shape differences. Symbol u_k and v_k are used for system stability analysis and will be described next. A logic switch signal K is the output signal of Λ. Q is a cost function that determine the area of inaccurate points. If Q is less than a threshold E_{th}, the switch k will be closed and the iteration process will be stopped, the current point cloud can then be sent out for comparison with its CAD model M.

The mathematic models of a point cloud Pc, a point cloud generator Γ and an error map generator Δ, shown in Figure 6 have been introduced in details in [11].

Equation (12) describes the model of the dynamic view planning process in a state space: V and Pc are state variables, M and TC are inputs, and error map E is the output of the system:

$$\begin{cases} V &\doteq f_0(M, TC) \cup g_k(IA) \\ Pc &\doteq \Gamma(V) \\ E &= \Delta(M, Pc) \end{cases} \quad (12)$$

where $\doteq$ indicates that V and Pc are accumulated results from iterations. As shown in Figure 6, given a CAD model M and a set of task constraints TC, a group of viewpoints V_0 will be initialized first, a point cloud Pc is then generated according to V_0. Initially, V is equal to V_0. Two functions Γ and Λ are then going to be executed based on this viewpoint set V. As described previously, Γ is an execution to obtain point clouds Pc from set V. Meanwhile, function Λ evaluates the current viewpoint by detecting regions of inaccurate points. If necessary, a group of new viewpoints can then be generated through function g_k.

IV. Experimental Implementation and Results

A 3D area sensor is developed and attached to an ABB robot in our laboratory, the system can be seen in Figure 8.

Fig. 8. Robot-aided Automatic 3D Rapid Surface Inspection System

The 3D area sensor is made by a LED-based DLP projector and a CCD camera. The weight is about five pounds, include the aluminum shield. The LED projector use a rechargeable battery as power source that can be continuously used for four hours. Both the camera and the projector are connected to a computer, which has a Matrox 1394 frame grabber, robot planning software, robot control software, and 3D measurement and inspection software installed. A part pillar (model number m32510) is provided by FORD Motor Company for experimental trials. The projected stripes and the point cloud on that view point is shown in Figure 9. Figure 10 displays all 16 point clouds measured over the part surface. A color coded map, also called error map, can be seen in Figure 11. The distribution of the color represents the shape variation between the profile of the real part surface and the desired shape, its CAD model.

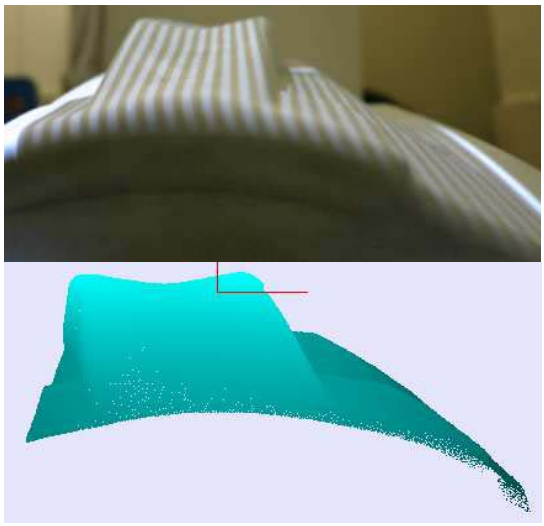

Fig. 9. Stripes and the correspondent point cloud from another view

The developed robot sensing system is also extended to rapid windshield dimensional inspection for the automotive glass industry. Because the worldwide competition, car makers increase the demand on the quality of the windshield's 3D shape. The traditional windshield bending process of the automotive glass industry needs a rapid 3D shape evaluation system as a feedback to the temperature control system. Traditional CMM technique cannot provide such online measurement and realtime feedback information. Non-contact 3D inspection technology then provides a solution to this requirement. Figure 12 illustrates an example of such an application, which is based on the robotic 3D inspection system.

Fig. 10. Point clouds measured on each viewpoint

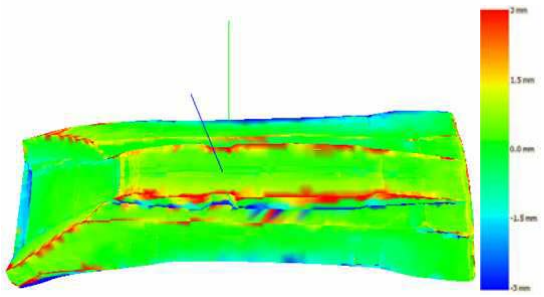

Fig. 11. The developed error map of pillar, m32510

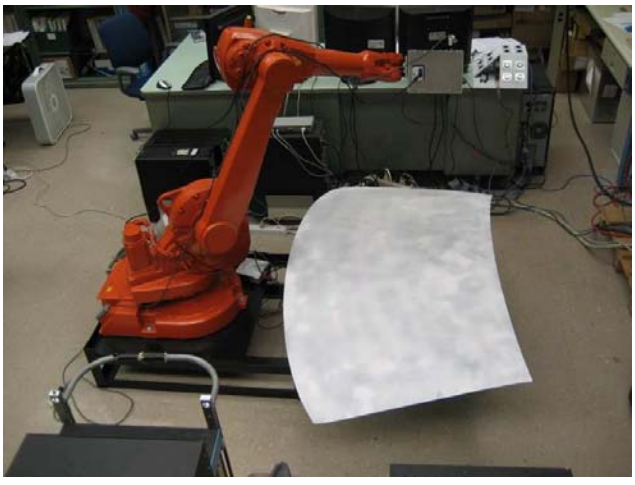

Fig. 12. Automatic 3D Rapid Windshield Inspection System

Figure 13 shows an errormap developed using traditional CMM technique, it usually takes two operators entire day to setup the windshield, calibrate measurement system, measure the surface, and then compare to the CAD model. The robotic measurement system, using online calibration technique, only needs three minutes to scan the whole piece surface and about two minutes to calculate the error map. In another aspect, the point density developed using CMM technique is much lower than rapid 3D inspection system. It is 25mm between each point in the sample errormap in Figure 13. Instead, the automatic 3D rapid inspection system, can reach to 0.2mm between each point. With this high point density, the surface geometry property, which includes the required 3D profile information, can be calculated directly. As a comparison of the errormap, the developed errormap is shown in Figure 14. Recently, our research extends to 3D shape measure of unpainted windshields. A recursive based back-imaging method has been developed for a new type of 3D area sensor, which is introduced in another paper. However, the feedback robot planning method, as a theoretical foundation, can be applied to the back-imaging approach as well. Results will be presented in the near future.

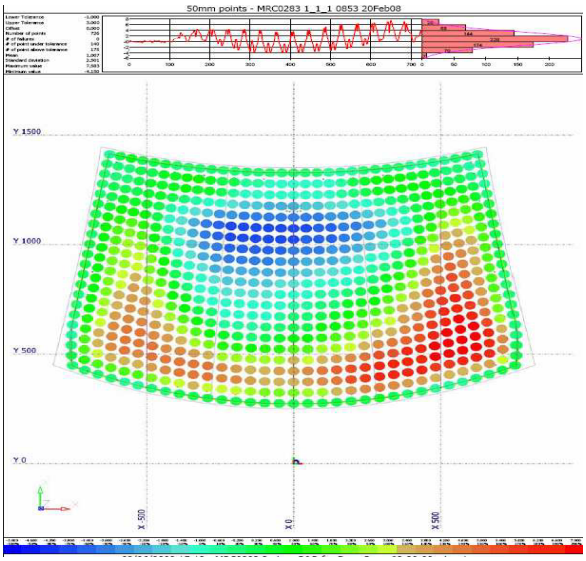

Fig. 13. The errormap of a windshield, developed by traditional CMM technique

V. CONCLUSIONS

In this paper, our current results on a feedback based robot area sensing system is presented. This system is developed for 3D shape quality control in the automotive industry. The feedback visual controller is used to improve the accuracy of a vision-based 3D shape measurement. CAD-guided planning is an effective way to estimate a group of view points for a 3D area sensor. However, image quantization error and poor surface reflection property may increase the measurement uncertainties, which cannot be solved by a CAD-guided robot sensor planning system.

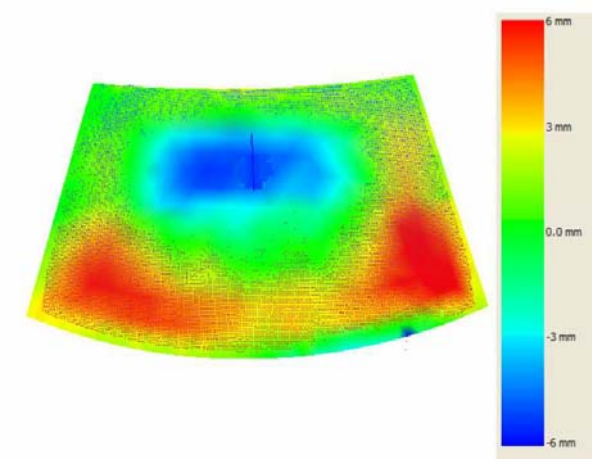

Fig. 14. The errormap of a windshield, developed by the automatic robot-aided inspection system

Feedback planning methods are developed to optimize the robot planner. Standard deviation between two point clouds is used to evaluate the quality of the measured point cloud. The point cloud obtained from this feedback system can be output directly for shape verification. Mathematical models of this system are developed. Experiments on an automotive body part and a glass windshield show the effectiveness of the designed automatic rapid surface inspection system.

REFERENCES

[1] Nello Zuech, *3D-Based Machine Vision in Automotive Production Lines*, http://www.machinevisiononline.org/public/articles/details.cfm?id=3415, 2007.

[2] T. S. Newman, A. K. Jain, *A Survey of Automated Visual Inspection* , Computer Vision and Image Understanding, Vol. 61(2), pp. 231-262, 1995.

[3] W. R. Scott, G. Roth, J. F. Rivest, *View Planning for Automated Three-Dimensional Object Reconstruction and Inspection*, ACM Computing Surveys, Vol. 35(1), pp. 64-96, 2003.

[4] S. Y. Chen and Y. F. Li, *Automatic Sensor Placement for Model-Based Robot Vision*, IEEE Transactions on System Man and Cybernetics, Part B, Vol. 34(1), pp. 393-408, 2004.

[5] X. Qian and K. G. Harding, *A Computational Approach for Optimal Sensor Setup*, SPIE Journal Optical Engineering, Vol. 42(5), pp. 1238-1248, May 2003.

[6] G. Impoco, P.Cignoni, and R.Scopogno, *Closing Gaps by Clustering Unseen Directions*, International Conference on Shape Modeling and Applications, pp. 307-316, 2004.

[7] B. Kamgar-Parsi and B. Kamgar-Parsi, *Evaluation of quantization error in computer vision* IEEE Transactions on Pattern Analysis and Machine Intelligence, vol. 11, Sept. 1989.

[8] S. D. Blostein and T. S. Huang, *Error analysis in stereo determination of 3-D point positions* IEEE Transactions on Pattern Analysis and Machine Intelligence, vol. 9, Nov, 1987.

[9] C. C. Yang, M. M. Marefat, and F. W. Ciarallo, *Error analysis and planning accuracy for dimensinal measurement in active vision inspection*, IEEE Transactions on Robotics and Automation, Vol. 14, NO. 3 June 1998.

[10] Q. Shi, N. Xi, H. Chen, Y. Chen, *Integrated Process for Measurement of Free-Form Automotive Part Surface Using a Digital Area Sensor*, IEEE International Conference on Robotics and Automation, pp. 580-585, 2005.

[11] Q. Shi, N. Xi, W. Sheng, and Y. Chen, *Development of Dynamic Inspection Methods for Dimensional Measurement of Automotive Body Parts*, IEEE International Conference on Robotics and Automation, Accepted, 2006.